BUTTERWORTH HEINEMANN

Forced convection from an isolated heat source in a channel with porous medium

Hyung Jin Sung, Seo Young Kim, and Jae Min Hyun
Department of Mechanical Engineering, Korea Advanced Institute of Science and Technology, Yusung, Taejon, South Korea

A numerical study is made of flow and heat transfer characteristics of forced convection in a channel that is partially filled with a porous medium. The flow geometry models convective cooling process in a printed circuit board system with a porous insert. The channel walls are assumed to be adiabatic. Comprehensive numerical solutions are acquired to the governing Navier–Stokes equations, using the Brinkman–Forchheimer-extended Darcy model for the regions of porous media. Details of flow and thermal fields are examined over ranges of the principal parameters; i.e., the Reynolds number Re, the Darcy number Da ($\equiv K/H^2$), the thickness of the porous substrate S, and the ratio of thermal conductivities R_k ($\equiv k_{eff}/k$). Two types of the location of the porous block are considered. The maximum temperature at the heat source and the associated pressure drop are presented for varying Re, Da, S, and R_k. The results illustrate that as S increases or Da decreases, the fluid flow rate increases. Also, as R_k increases for fixed Da, heat transfer rates are augmented. Explicit influences of Re on the flow and heat transport characteristics are also scrutinized. Assessment is made of the utility of using a porous insert by cross comparing the gain in heat transport against the increase in pressure drop.

Keywords: porous block in a channel; forced convection; heat transfer; pressure drop

Introduction

With the advent of high-performance electronic devices, efficient removal of increased heat generation from the system has emerged as a crucial task (Kraus and Bar-Cohen 1983). A large body of technical literature exists for electronic packaging and cooling problems. Much of the current research focuses on heat transports by means of convective fluid flows. A central theme of these studies is the question of how to effectuate increased heat transfers for given flow geometry and under externally imposed physical constraints (Davalath and Bayazitoglu 1987; Incropera 1988; Kang et al. 1990; Kennedy and Zebib 1983; Kim et al. 1992).

As a means toward realizing enhanced heat transfer, the effectiveness of using saturated porous media in the convective fluid flow system has been recognized for some time (Cheng et al. 1988; Combarnous and Bories 1975; Kaviany 1985; Kaviany 1991; Poulikakos and Bejan 1985; Poulikakos and Renken 1987; Lauriat and Prasad 1989; Vafai and Tien 1981). Technological applications in which porous materials are utilized include geophysical fluid engineering, thermal insulation, and solid-matrix heat exchangers. Recent efforts emphasize new approaches to enhanced heat transfer applications in electronic cooling problems by introducing porous media in the convective system (Hadim 1994; Huang and Vafai 1994; Hunt and Tien 1988; Kim and Vafai 1990; Tong and Sharatchandra 1990).

In an earlier treatise, Hunt and Tien (1988) demonstrated the feasibility of heat transfer augmentation by use of a foam material product. Vafai and Kim (1990) and Huang and Vafai (1994) investigated forced convection over an external boundary that was coated with a porous substrate. Vafai and Huang (1993, 1994) considered the effect of using intermittently porous cavities and of discrete porous block on an external plate. Hadim (1994) conducted a numerical study of forced convection in a porous material-filled channel that contained discrete heat sources. An important finding was made by Tong and Sharachandra (1990) where in the use of only a slice of porous material inserted in the channel could lead to a considerable augmentation of convective heat transfer. This has significant implications. To achieve heat transfer enhancements, the entire interior of the channel need not be completely filled with a porous medium. Substantial gains in heat transports can still be anticipated when only portions of the channel interior are filled with porous material. The effectiveness of a partially porous-filled convective system has other important advantages. The placement of porous media inside a fluid passageway produces resistance to the flow, which results in the form of a pressure loss in the downstream locations. This is the penalty that has to be overcome by an increased pumping power to maintain the flow. The employment of a partially porous channel brings an additional benefit, because the pressure drop over the channel length is smaller than for the case of a completely porous channel. The idea of using a partially porous channel was extended by Huang and Vafai (1994b), wherein a multiple porous structure was attached to the channel wall.

It is noted that most earlier studies involving porous/fluid composite systems have dealt with forced convection problems. Little attention has been given to heat transfer by forced convection from an isolated heat source in a confined passageway partially filled with porous media. As mentioned earlier, Tong and

Address reprint requests to Prof. Hyung Jin Sung, Dept. of Mechanical Engineering, Korea Advanced Inst. of Science and Technology, Yusung, Taejon, 305–701, South Korea.

Received 13 November 1994; accepted 18 May 1995

Int. J. Heat and Fluid Flow 16: 527–535, 1995

655 Avenue of the Americas, New York, NY 10010

0142-727X/95/$10.00
SSDI 0142-727X(95)00032-L

Sharatchandra (1990) and Huang and Vafai (1994b) reported the effect of thickness of porous substrate on the heat transfer rates from a constant temperature wall in a channel. It will be useful to perform further, systematic studies on the effects of interior shape of the channel, the thickness of porous substrate, and the thermal conductivity ratio of porous medium. In particular, the overall gain in heat transfer should be carefully weighed in light of the increased pressure drop, because these adjustable system parameters vary. The present paper addresses this point.

To concentrate on the impact of the presence of porous materials, a simple prototypical flow configuration is selected in the present work. A single block of porous material is placed inside a channel. The finite size, location, and physical properties of this block constitute the principal design parameters. Numerical solutions of the full, elliptic Navier–Stokes equations are acquired in the forced-convection parameter regime. In an effort to provide a guide in realistic application, optimal operating conditions of the system are sought. These would lead to a maximum enhancement of heat transfer, as well as a minimum loss of pressure in the downstream. Comprehensive flow and heat transfer characteristics are delineated as the Reynolds number and Darcy number encompass ranges of practical interest. Also, we scrutinize the effects of the location and size of the porous block on the global transport processes.

We mention the principal geometric differences between the present model and the previous accounts. Tong and Sharachandra (1990) considered a long porous insert that occupies the central portion of the entire channel length [see Figure 1(a)]. The channels wall were isothermal, and no heat sources were considered. In the case of Hadim (1994), several discrete porous bands, with finite width, were employed. Each porous band fills the entire cross section of the channel [see Figure 1(b)]. Huang and Vafai (1994b) examined the flow when several finite-sized blocks were placed attached to one channel wall [Figure 1(c)]. The entire channel walls were isothermal, and no heat sources were included in the system. As demonstrated in Figures 1(d) and (e) of the present study, the flow and transport properties are very sensitive to the geometric configurations and arrangement of the porous materials. The aim of the present work is to explore the specific parameter dependence of the heat transfer enhancement characteristics on the geometric particulars and arrangement of a single isolated porous block placed over a heating zone in the channel.

Mathematical formulation and numerical approach

The basic set up of the present flow model, shown in Figures 1(d) and (e), if the porous blocks are removed, is paradigmatic of a horizontal channel passageway with a discrete heating element embedded on the bottom surface wall. This configuration was treated previously by Kennedy and Zebib (1983). In the present case, a porous block of finite dimension is added to the system. As stressed earlier, changes in flow structure and possible augmentations in attendant heat transfer caused by the presence of a porous block are to be delineated. Two types of interior shape of the channel are considered for detailed analysis: (1) when the porous block is attached to the upper surface wall vertically above the heating zone, referred to as type (A) [Figure 1(d)]; and (2) when the porous block is attached to the heating zone on the bottom surface wall, denoted by type (B), [Figure 1(e)]. These two types are intended to highlight the importance of the size and location of the porous block in augmenting heat transports. In this work, the flow is assumed to be steady, incompressible, laminar, and two-dimensional (2-D). The geomtric particulars of the channel, heating zone, and porous block are shown in Figures 1(d) and 1(e). It is noted that the configuration of Figure 1(e) is somewhat impracticable in electronic chip cooling. The intension here is to run parameter studies to deepen an understanding of the conceivable flow configurations. The inlet fluid temperature T_{in} is assumed to be constant. The thermophysical properties of the fluid and the porous matrix are taken to be constant. In addition, the fluid-saturated porous medium is considered to be homogeneous, isotropic, and in local thermodynamic equilibrium with the fluid (Hadim 1994; Huang and Vafai 1994b; Tong and Sharatchandra).

The fundamental equations governing the fluid-porous system have been established under several physically plausible assumptions and relevant empirical relations. The Brinkman–Forchheimer-extended Darcy model is adopted for the porous region (Vafai and Tien 1981). This formulation takes into account both viscous and inertia effects. The present approach is advantageous, because a single set of governing equations is applicable to both fluid and porous regions, with proper interpretations of the physical variables. It is remarked that the one-equation approach may not yield correct results in conventional finite-difference treatment. However, by using a control-volume-based method, such as that employed here, the interface matching conditions are satisfactorily dealt with (Patankar 1980; Berkerman et al. 1988). Justification for this approach has been thoroughly checked in the preparation stage (Hadim 1994; Huang and Vafai 1994b). The equations, in dimensionless form, are as follows:

$$\nabla \cdot \mathbf{V} = 0, \tag{1}$$

$$\mathbf{V} \cdot \nabla U = -\frac{\partial P}{\partial X} + \frac{2}{\mathrm{Re}} \nabla^2 U - \zeta \left[\frac{2\varepsilon}{\mathrm{Da} \cdot \mathrm{Re}} + \frac{C \cdot \varepsilon^2}{\sqrt{\mathrm{Da}}} |\mathbf{V}| \right] U, \tag{2}$$

Notation

C_p specific heat of fluid
D_h hydraulic diameter for the channel, $2H$
H height of flow channel
k thermal conductivity of fluid
l length of heat source
l_1 length of upstream section from an isolated heat source
l_2 length of downstream section from an isolated heat source
L, L_1, L_2 dimensionless lengths, l/H, l_1/H, l_2/H
L_T dimensionless length, $L_1 + L + L_2$
p pressure
s dimensional thickness of porous substrate
S dimensionless thickness of porous substrate, s/H
T dimensional temperature
u, v dimensional velocity components
U, V dimensionless velocity components, u/U_{in}, v/U_{in}
x, y dimensional axial and transverse coordinates
X, Y dimensionless axial and transverse coordinates, x/H, y/H

Greek

α thermal diffusivity, $k/(\rho C_p)$
ε porosity of porous medium
ν kinematic viscosity
ρ density
ψ stream function

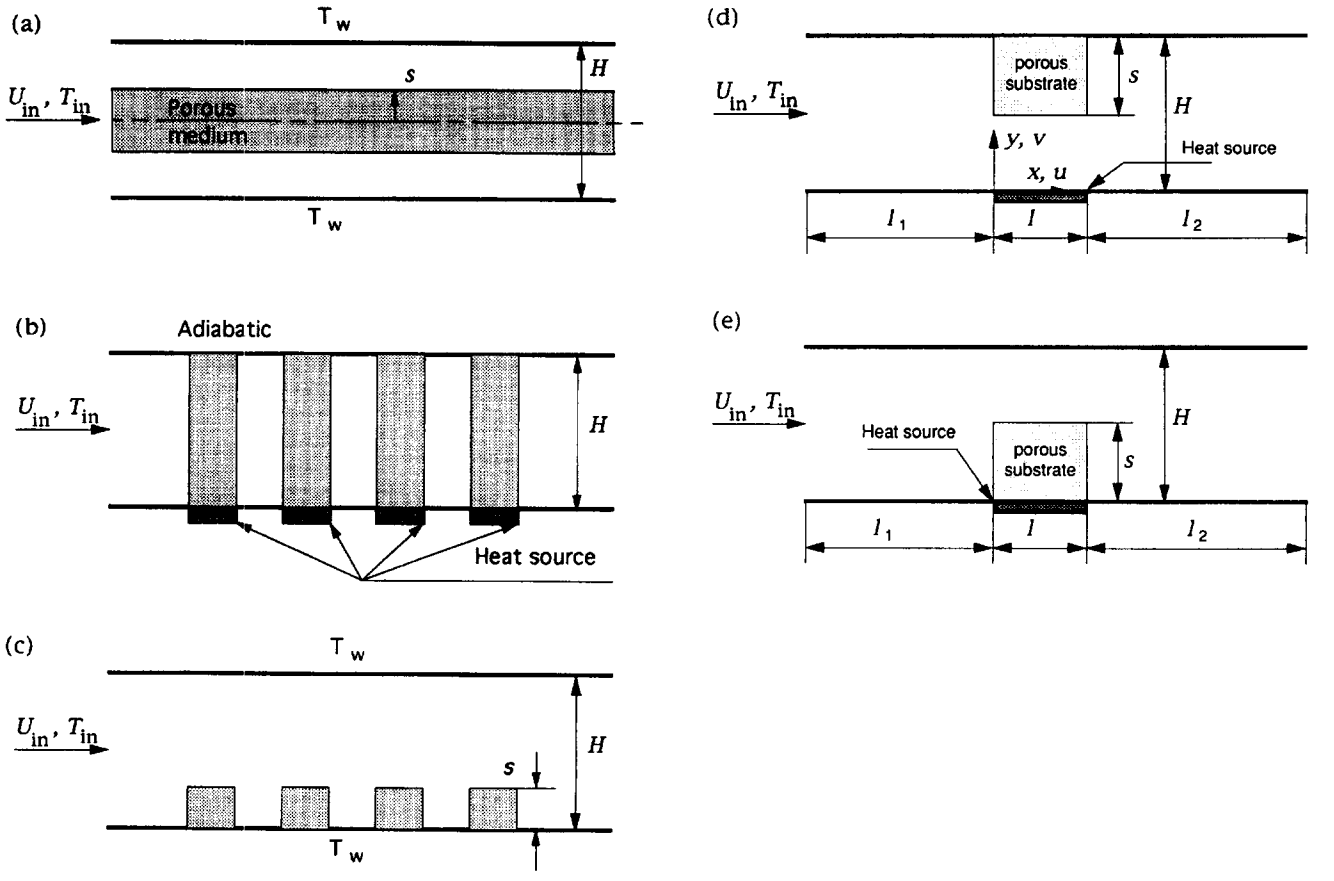

Figue 1 Schematic flow configuration and arrangement of porous materials (a) model of Tong and Sharatchandra (1990); (b) model of Hadim (1994); (c) model of Huang and Vafai (1994); (d) the present model, type (A); and (e) the present model, type (B)

$$\mathbf{V}\cdot\nabla V = -\frac{\partial P}{\partial Y} + \frac{2}{\mathrm{Re}}\nabla^2 V - \zeta\left[\frac{2\varepsilon}{\mathrm{Da}\cdot\mathrm{Re}} + \frac{C\cdot\varepsilon^2}{\sqrt{\mathrm{Da}}}|\mathbf{V}|\right]V, \tag{3}$$

$$\mathbf{V}\cdot\nabla\theta = [(R_k-1)\zeta+1]\frac{2}{\mathrm{Re}\cdot\mathrm{Pr}'}\nabla^2\theta, \tag{4}$$

in which $\mathbf{V}$ represents the fluid velocity in the fluid region, and, in the porous region, $\mathbf{V}$ denotes the Darcian (filtration) velocity; Pr′ denotes the modified Prandtl number; i.e., εPr, where ε is the porosity. In the equations, the fluid-occupied region $\varepsilon = 1.0$ is identified by setting the index $\zeta = 0$, and the porous region is tagged by $\zeta = 1.0$. In the present paper, $\varepsilon = 0.9$ is used for the porous medium (Kaviany 1991). The dimensionless quantities are as follows:

$$X \equiv \frac{x}{H}, Y \equiv \frac{y}{H}, \mathbf{V} \equiv \frac{\mathbf{v}}{\varepsilon\cdot U_{\mathrm{in}}}, P \equiv \frac{p}{\rho U_{\mathrm{in}}^2}, \theta \equiv \frac{T-T_{\mathrm{in}}}{q''H/k}, \tag{5}$$

in which U_{in} and T_{in} denote the average velocity and temperature at the entrance q'' the heat flux from the heated element, and k the thermal conductivity of the fluid. The nondimensional parameters are as follows:

Reynolds number:

$$\mathrm{Re} = U_{\mathrm{in}}D_h/\nu \tag{6}$$

Prandtl number:

$$\mathrm{Pr} = \nu/\alpha \tag{7}$$

Darcy number:

$$\mathrm{Da} = K/H^2 \tag{8}$$

Thermal conductivity ratio:

$$R_k = k_{\mathrm{eff}}/k \tag{9}$$

In the above, $\alpha_{\mathrm{eff}} = k_{\mathrm{eff}}/(\rho C_p)$, and k_{eff} represents the effective thermal conductivity of the porous medium; C and K denote, respectively, the inertia coefficient and the permeability. The value of C in Forchheimer's extension is taken to be a constant, and in line with the suggestions of Beckerman et al. (1988), it is set $C = 0.55$. The value of ν is adopted in the present study as an approximated value of ν_{eff}, while the value of ν_{eff} in Brinkman's extension in the momentum equation remains controversial (Lundgren 1972). This value is used in all calculations in this paper.

The proper boundary conditions are now stipulated. No-slip conditions are applied at the solid surface of the base plates of the channel:

$$U(X,Y) = V(X,Y) = 0 \quad \text{on} = 0, 1, \quad \text{for} \quad -L_1 < X < L + L_2, \tag{10}$$

In many real applications, the flow at the inlet may not be fully developed. However, in the present account, a fully developed parabolic flow is assumed at the channel inlet. By this choice, the effect of variation of the entrance length L_1 is eliminated, which is not a major issue in the present analysis. This procedure is in line with the approaches of Davalath and Bayazitoglu (1987) as well as of Huang and Vafai (1994b).

$$U(-L_1, Y) = 6(Y - Y^2), V(-L_1, Y) = 0, \quad \text{for} \quad 0 < Y < 1 \tag{11}$$

As stated earlier, the temperature at the inlet is uniform:

$$\theta(-L_1, Y) = 0, \qquad \text{for} \qquad 0 < Y < 1 \tag{12}$$

The surfaces of the channel walls are thermally insulated (Kennedy and Zebib 1983).

$$\frac{\partial\theta}{\partial Y}(X, Y) = 0 \quad \text{on} \quad Y = 0, 1 \quad \text{for} \quad -L_1 < X < L + L_2 \tag{13}$$

For the zone of heat source ($0 < X < L$), a uniform heat flux is specified:

For type (A):

$$\frac{\partial\theta}{\partial Y}(X, 0) = -1$$

For type (B):

$$\frac{\partial\theta}{\partial Y}(X, 0) = -\frac{1}{R_k} \tag{14}$$

The downstream length of the channel is assumed to be sufficiently long to ensure that fully developed conditions are applicable at the exit (Davalath and Bayazitoglu 1987; Hadim 1994; Kim et al. 1992); i.e.

$$\frac{\partial\Phi}{\partial X}(L + L_2, Y) = 0, (\Phi = U, V, \theta), \quad \text{for} \quad 0 < Y < 1 \tag{15}$$

The system of equations above is solved numerically by using the well-documented SIMPLER algorithm of Patankar (1980). This is based on a control-volume formulation, which ensures conservation of mass, momentum, and heat fluxes across the control surfaces and, thus, across the fluid/porous-medium interface as well. A harmonic-mean formulation is adopted for the interface diffusion coefficients between two control volumes, and this approach is capable of handling abrupt changes in these coefficients at the fluid/porous interface (Patankar 1980). The convection terms in the governing equations are discretized by using a third-order upwind scheme (QUICK) on nonuniform grids (see Hayase et al. 1992). These procedures yield stable convergence with less numerical diffusion. Central differencing is applied to the diffusion transport terms. The resulting algebraic equations are solved by the tridiagonal matrix algorithm (Patankar 1980).

All computations were performed on a (140 × 50) grid network. In the X-direction, the mesh points were densely packed near the heat source. In the Y-direction, grid points were clustered near the top and bottom surfaces of the channel as well as in the neighborhood of fluid/porous medium boundaries. Convergence was declared when maximum relative variations in U, V, and θ between two successive iterations were less than 10^{-4}. Many trial calculations were repeated to test sensitivity of the results to grid size, and the outcome of these was satisfactory.

Results and discussion

In actual calculations, the geometrical particulars are set forth (Kennedy and Zebib 1983): $L = 1.0$, $L_1 = 5.5$, and $L_2 = 15.0$. Several exemplary calculations confirmed that the above values produce results compatible with the exit conditions adopted in the present study. In all computations, the Prandtl number was set $\mathrm{Pr} = 0.72$, and the Reynolds number was in the range $10 \sim 500$. The geometric shape of the channel and the parameter space covered are in line with the problem setup of preceding related studies (Kennedy and Zebib; Hadim 1994). The crux of the present investigation lies in the insertion of a finite-volume porous block into the channel. Consequently, crucial parameters relative to the porous block are the Darcy number ($10^{-6} \le \mathrm{Da} \le \infty$), the thickness of the porous substrate ($0 \le S \le 1$), and the thermal conductivity ratio ($0.1 \le R_k \le 10$).

In postprocessing the results, an important quantity is the overall pressure drop ΔP throughout the entire channel length. The pressure drop increases because of the presence of the porous block. In realistic engineering applications, this added pressure drop is the price that must be paid in return for the gain in heat transfer augmentation by inserting a porous block. The dimensional pressure drop can be expressed in terms of the friction factor f:

$$f = (-\Delta P / L_T) D_h / \left(\tfrac{1}{2}\rho U_{\mathrm{in}}^2\right) \tag{16}$$

where D_h is the hydraulic diameter of the channel cross section.

Before proceeding further, it is necessary to ascertain the reliability and accuracy of the present simulations. Toward this end, some of the qualitative characteristics of standard model flows, for which solutions have been documented, have been recapitulated. Suffice it to say that the present numerical results have been shown to be compatible with the available data. In ensuing developments, the numerical results will be systematically analyzed to disclose the influences of individual parameters involved.

Figure 2 exemplifies the global flow pattern for type (A) at $\mathrm{Re} = 100$. When S is small, the flow obstruction by the porous block is not pronounced, as anticipated. When the block size is large, the unobstructed fluid passing shrinks. The fluid flow is concentrated through the narrow opening between the block and the bottom surface of the wall. As demonstrated in Figure 2(b), at the immediate downstream locations of the block, an intense recirculation zone appears near the upper surface wall. A weaker cell is also visible at farther downstream locations near the bottom surface of the channel. This flow structure points to intensified convective activities near the wall, which brings forth increased heat transfer between the heat source and the fluid. However, when the porous block covers the entire cross section of the channel

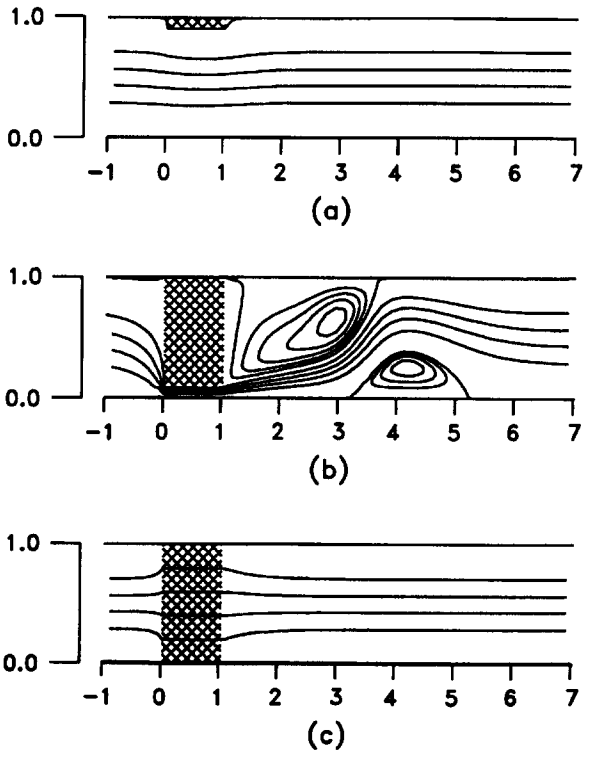

Figure 2 Flow patterns; $\mathrm{Re} = 100$ and $\mathrm{Da} = 10^{-5}$; contour intrerval $\Delta\Psi = 0.2$ for $0 < \Psi \le 1.0$; (a) $S = 0.1$; $\Psi_{\max} = 1.0$, and $\Psi_{\min} = 0.0$; (b) $S = 0.9$; $\Psi_{\max} = 1.459$, and $\Psi_{\min} = -0.036$; beyond $\Psi = 1.0$, contour interval $\Delta\Psi = 0.1$; below $\Psi = 0.0$, contour interval $\Delta\Psi = 0.01$, (c) $S = 1.0$; $\Psi_{\max} = 1.0$ and $\psi_{\min} = 0.0$

($S = 1.0$), the fluid moves through the block in a fairly uniform fashion. Notice that, for the cases of Figure 2, the externally prescribed value of Re as well as the thermophysical properties of the porous material are the same.

The effects of Re and of Da on the global flow pattern are shown in Figure 3. For fixed Da, the flow behind the block is intensified as Re increases [compare Figures 3(a) and 3(b)]; in particular, the recirculation zone behind the block becomes larger in size. At $Da = 10^{-5}$, the pictures in Figures 3(a) and 3(b) resemble the flows behind a completely solid block. The fluid flow rate passing through the porous block is very small. When Da is large [see Figure 3(c) for $Re = 500$, $Da = 10^{-2}$], the resistance to flow by the porous region is small, and, accordingly, the recirculation cell behind the porous block diminishes.

Figure 4 displays the detailed profile of U with Y for type (A) along a vertical cut through the midpoint of the block (at $X = 0.5$). The effect of the block size, at fixed Re and Da, is exhibited. Noted that, when S takes a large value close to 1.0 (see the curve for $S = 0.9$), the flow is concentrated to the unobstructed opening; i.e., $1 - S \leq Y \leq 1.0$, and, therefore, a strong velocity gradient $\partial u/\partial y$ is created in the vicinity of the lower surface of the channel. This points to a vigorous convective activity near the heat source, which leads to enhanced heat transfer between the heat source and the fluid. As illustrated earlier, when the porous block extends throughout the entire channel cross section ($S = 1.0$), the velocity in the interior core of the channel is small in magnitude and uniform in the Y-direction. This observation was also asserted by Tong and Sharatchandra (1990).

Because no buoyancy effects are included in the present analysis, the qualitative features of flow behavior do not exhibit major differences between type (A) and type (B). For type (B), the flow patterns are almost symmetrical to the patterns of type (A) with respect to the centerline of the channel $Y = 0.5$.

Figure 5 is typical of the thermal field in the entire channel for type (A), as Re and Da vary for fixed S and R_k. As Re increases at

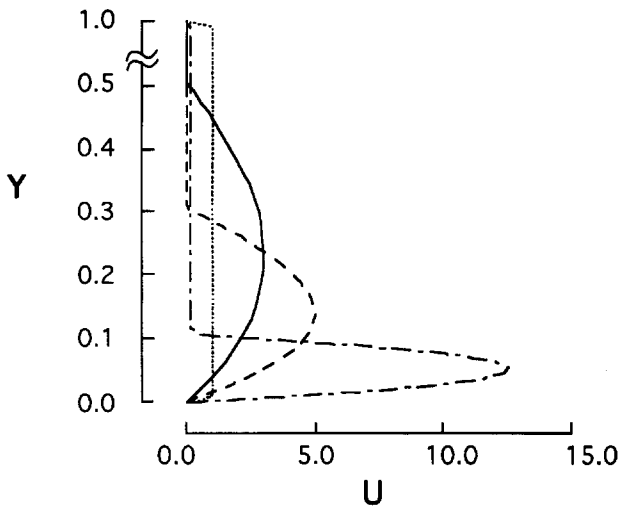

Figure 4 Plots of U-velocity profile at $X = L/2$ for varying S; $Re = 100$ and $Da = 10^{-5}$; ——, $S = 0.5$; - - - -, $S = 0.7$; — · —, $S = 0.9$; · · · · · · · · ·, $S = 1.0$

fixed Da [see Figure 5(a) and 5(b)], the concentration of heated fluid into a thin boundary layer becomes conspicuous. On the other hand, an increase of Da from $Da = 10^{-5}$ to $Da = 10^{-2}$ [see Figures 5(b) and 5(c)] causes only a marginal change in the thermal characteristics in the channel. It is seen that an increase in Re, by promoting convective activities, is an effective method to enhance heat transfer.

The impact of the size and location of the porous block is illustrated in Figure 6. Both Re and Da are fixed. As can be inferred from the velocity plot of Figures 2 and 4, the clustering of isotherms near the heat source is manifested as S changes from a

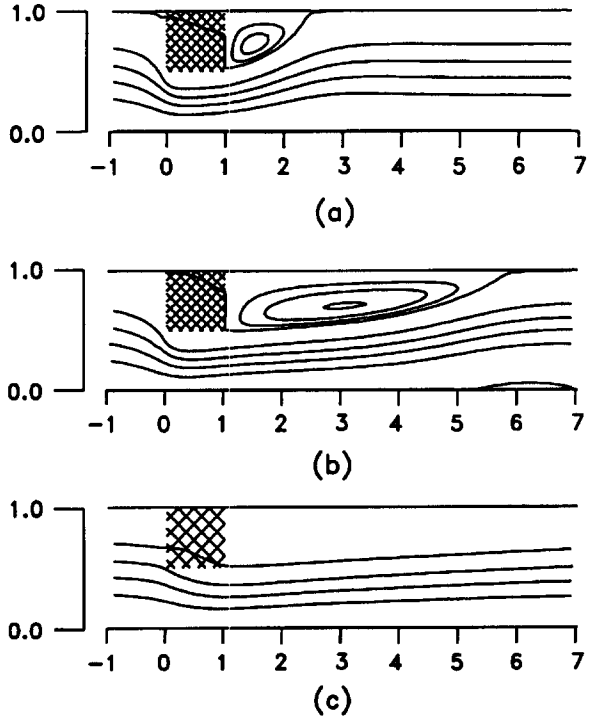

Figure 3 Flow patterns; $S = 0.5$; contour interval $\Delta\Psi = 0.2$ for $0 < \Psi < 1.0$; (a) $Re = 100$, $Da = 10^{-5}$; $\Psi_{max} = 1.050$; beyond $\Psi = 1.0$, contour interval $\Delta\Psi = 0.02$; (b) $Re = 500$, $Da = 10^{-5}$; $\Psi_{max} = 1.061$; beyond $\Psi = 1.0$, contour interval $\Delta\Psi = 0.02$; (c) $Re = 500$, $Da = 10^{-2}$; $\Psi_{max} = 1.0$

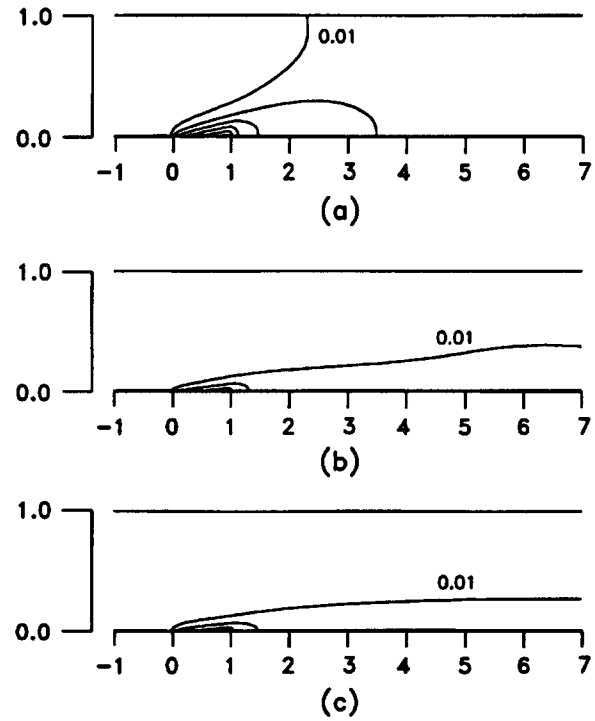

Figure 5 Plots of isotherms for type (A); $S = 0.5$ and $R_k = 1.0$; contour interval $\Delta\Theta = 0.03$ beginning with $\theta = 0.01$; (a) $Re = 100$, $Da = 10^{-5}$; (b) $Re = 500$, $Da = 10^{-5}$; (c) $Re = 500$, $Da = 10^{-2}$

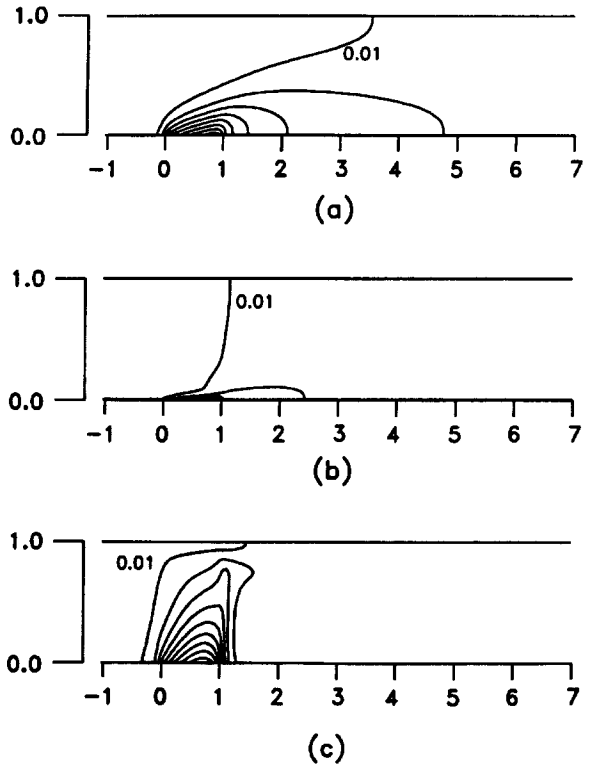

Figure 6 Plots of isotherms; Re = 100, Da = 10^{-5}, and $R_k = 1.0$; (a) type (A), $S = 0.1$; contour interval $\Delta\theta = 0.03$ beginnig with $\theta = 0.01$; (b) type (A), $S = 0.09$; contour interval $\Delta\theta = 0.02$ beginning with $\Theta = 0.01$; (c) type (B), $S = 0.9$; contour interval $\Delta\theta = 0.03$ beginning with $\Theta = 0.01$

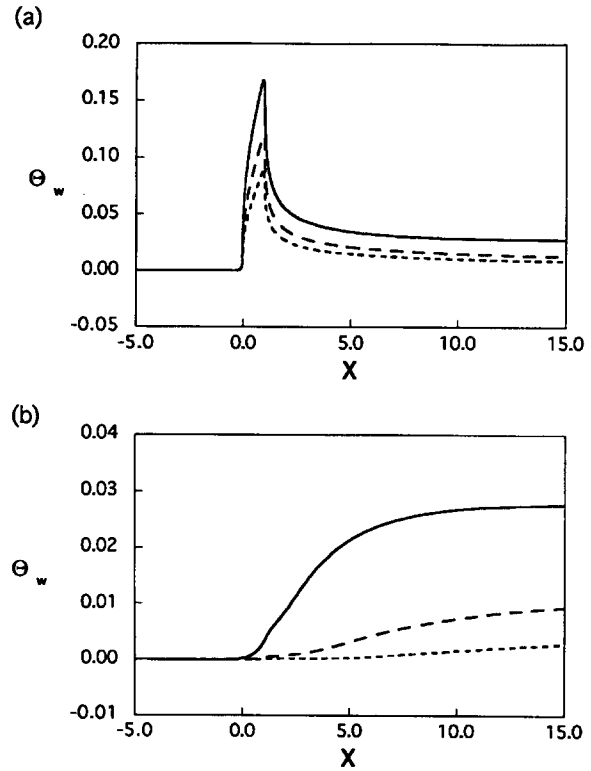

Figure 7 Surface temperature Θ_w profiles for type (A); Da = 10^{-5}, $S = 0.5$, and $R_k = 1.0$; (a) on the lower surface wall ($Y = 0$); (b) on the upper surface wall ($Y = 1.0$); ————, $Re = 100$; – – – –, Re = 250; ———————, Re = 500

low value [$S = 0.1$ in Figure 6(a)] to a high value [$S = 0.9$ in Figure 6(b)]. This clearly demonstrates that a high value of S results in a narrow, unobstructed fluid passageway, which gives rise to an augmented heat transfer process. When $S = 0.9$, the changes between type (A) and type (B) are shown in Figures 6(b) and (c). For type (B), it is seen that the isotherms are more spread out in the cross section above the heat source, as compared to the case of type (A). Within the porous block, the fluid velocities for type (B) are small, and the temperatures tend to be more equally distributed. This tends to reduce the effectiveness of transport process between the fluid and the channel walls.

The local temperature Θ_w at the channel walls is portrayed in Figure 7 for type (A), for fixed Da, S, and R_k. Substantial variations in Θ_w are seen at the lower channel wall in the region of heat source. On the upper channel wall, Θ_w-variations are more gradual in the regions downstream of the block. Figure 7 clearly depicts the efficiency of transfer processes, which may be measured in terms of the magnitude of Θ_w. If the formulation is translated into the physical problem of an electronic device cooling, reduction of $(\Theta_w)_{max}$ below a certain allowable limit is essential. The lowering of $(\Theta_w)_{max}$ with increasing Re is apparent. Note the difference in scales of the ordinates of Figures 7(a) and (b).

Similar pictures are shown in Figure 8 for type (B). It should be pointed out that Θ_w near the heat source at the bottom wall is substantially higher for type (B) than for type (A) [note the difference in scales in the ordinates of Figures 7(a) and 8(a)]. However, Θ_w profiles at the upper channel wall do not display many quantitative changes between type (A) and type (B).

The effect of Da on Θ_w is illustrated in Figure 9 for type (A) and in Figure 10 for type (B). For type (A), as Da decreases, near the

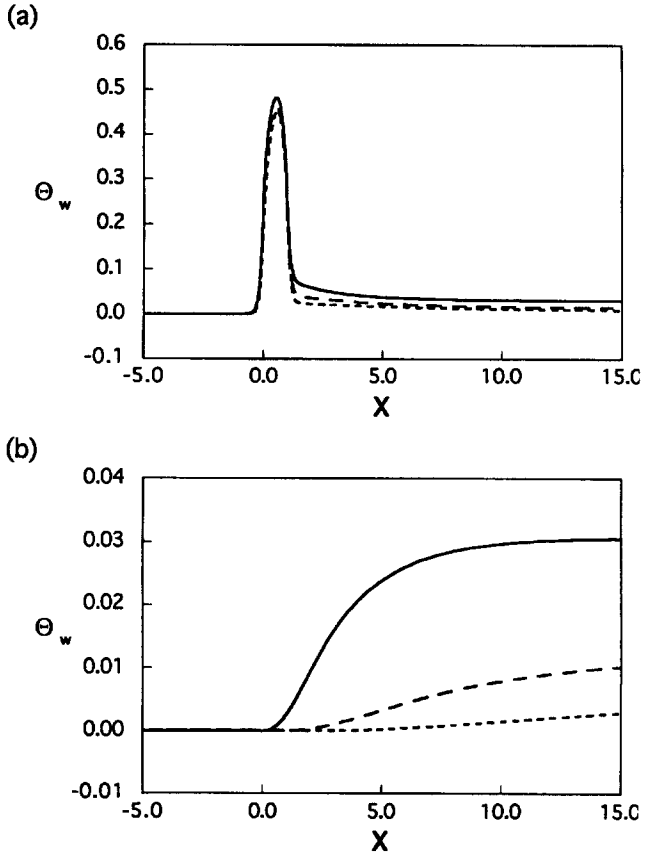

Figure 8 Surface temperature Θ_w profiles for type (B); Da = 10^{-5}, $S = 0.5$, and $R_k = 1.0$; (a) on the lower surface wall ($Y = 0$); (b) on the upper surface wall ($Y = 1.0$); ——, $Re = 100$; — — —, Re = 250; – – –, Re = 500

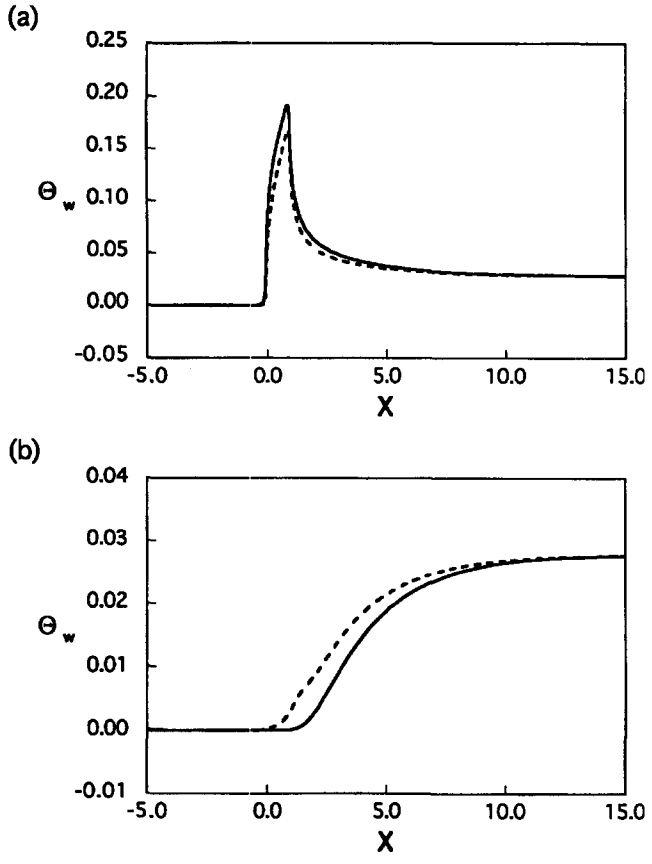

Figure 9 Surface temperature Θ_w profiles for type (A); Re = 100, $S = 0.5$, and $R_k = 1.0$; (a) on the lower surface wall ($Y = 0$); (b) on the upper surface wall ($Y = 1.0$); ——, $Da = 10\&SUP-2$; – – –, $Da = 10^{-6}$

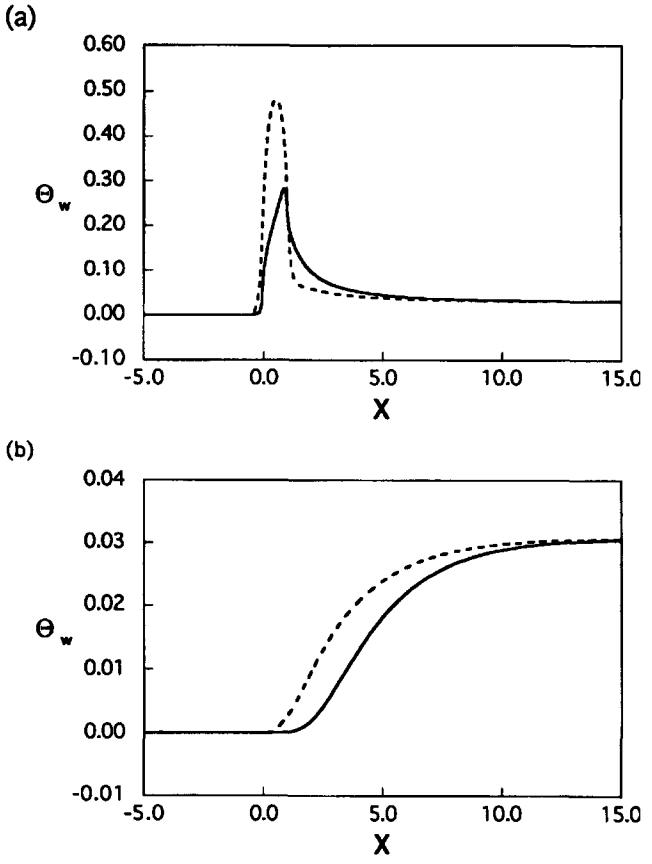

Figure 10 Surface temperature θ_w profiles for type (B); Re = 100, $S = 0.5$, and $R_k = 1.0$; (a) on the lower surface wall ($Y = 0$); (b) on the upper surface wall ($Y = 1.0$); ——, $Da = 10^{-2}$ – – –, $Da = 10^{-6}$

heat source and at its downstream locations, Θ_w at the lower channel wall decreases; whereas, Θ_w at the upper channel wall increases. This is attributable to the role of the recirculating cell that exists immediately behind the porous block. When the block is of low permeability (Da decreases to a small value; i.e., $Da = 10^{-6}$), the block behaves more like a solid, thereby generating a stronger recirculation zone. However, for type (B), the decrease of Da results in an increase of Θ_w at the heat source. This is attributed to the weaker convective heat transfer near the heat source by using a low-permeability material. Θ_w at the upper channel wall for type (B) shows a similar trend to that of type (A).

As stressed earlier, from the standpoint of industrial applications, the attainment of $(\Theta_w)_{max}$ below a certai permissible value is a primary goal. However, consideration has to be given to the associated pressure drop that occurs because of the presence of the porous block.

The pressure drop will be expressed in terms of $f\mathrm{Re}/(f\mathrm{Re})_o$, where $(f\mathrm{Re})_o$ indicates the value when no porous block is employed. As is well kwown (Kays and Crawford 1980), $(f\mathrm{Re})_o = 24.0$. In the ensuing plots, variations of $(\Theta_w)_{max}$ and of $f\mathrm{Re}$ are displayed as the principal parameters vary.

Figure 11 shows the impact of S. For type (A), $(\Theta_w)_{max}$ has a minimum around $S \sim 0.9$, which is consistent with the findings of Tong and Shararatchandra (1990). For type (B), as S increases, $(\Theta_w)_{max}$ increased to a maximum around $S \sim 0.7$, and $(\Theta_w)_{max}$ decreases afterward. The pressure drop increases substantially as S increases to values close to $S \sim 1.0$. Notice that, when $S = 1.0$, the pressure drop is more than 400 times the value of a nonporous channel. This is suggestive of an extremely high price, in terms of the pumping requirement, that is attendant in utilizing a porous material.

The effect of Re is depicted in Figure 12. As Re increases, $(\Theta_w)_{max}$ decreses, as expected. The trend is similar for both type (A) and type (B), although the magnitude of $(\Theta_w)_{max}$ is higher for type (B) than for type (A). The pressure drop increases almost linearly with Re.

Figure 13 demonstrates the influence of Da on $(\Theta_w)_{max}$ and on $f\mathrm{Re}$. For type (A), as Da decreases, $(\Theta_w)_{max}$ gradually decreases.

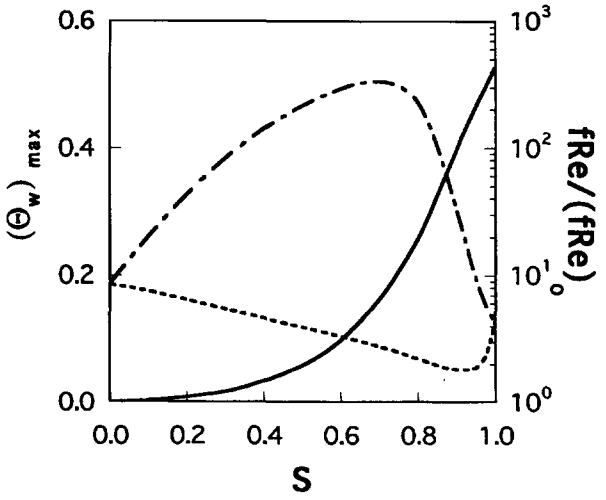

Figure 11 Plots of maximum wall temperature $(\Theta_w)_{max}$ and attendant pressure drop ratio $f\mathrm{Re}/(f\mathrm{Re})_o$; Re = 250; $Da = 10^{-5}$, and $R_k = 1.0$; $(\theta_w)_{max}$: ——, type (A); — — —, type (B); $f\mathrm{Re}/(f\mathrm{Re})_o$: – – –

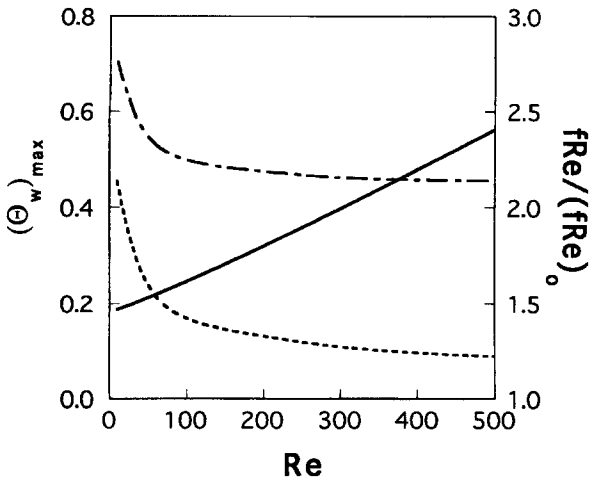

Figure 12 Plots of maximum wall temperature $(\theta_w)_{max}$ and attendant pressure drop ratio $f\text{Re}/(f\text{Re})_o$; Da $=10^{-5}$, S $=0.5$, and $R_k=1.0$; $(\theta_w)_{max}$: – – –, type (A); — · —, type (B); $f\text{Re}/(f\text{Re})_o$: ——

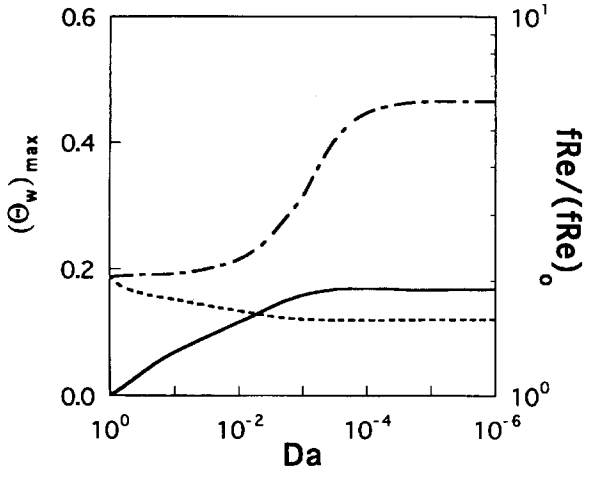

Figure 13 Plots of maximum wall temperature $(\theta_w)_{max}$ and attendant pressure drop ratio $f\text{Re}/(f\text{Re})_o$; Re $=250$, S $=0.5$, and $R_k=1.0$; $(\theta_w)_{max}$: – – –, type (A); — · —, type (B); $f\text{Re}/(f\text{Re})_o$: ——

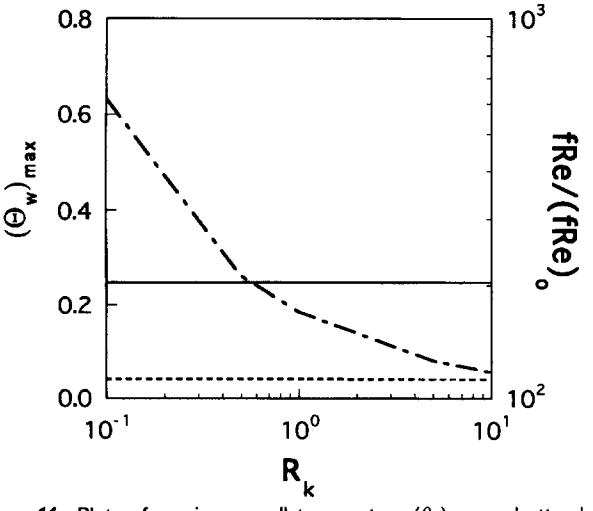

Figure 14 Plots of maximum wall temperature $(\theta_w)_{max}$ and attendant pressure drop ratio $f\text{Re}/(f\text{Re})_o$; Re $=250$, Da $=10^{-5}$, and $S=0.95$; $(\theta_w)_{max}$: – – –, type (A); — · —, type (B); $f\text{Re}/(f\text{Re})_o$: ——

For type (B), a decrease of Da results in a substantial increase of $(\Theta_w)_{max}$. It is noted that, when Da is smaller than Da $\sim 10^{-4}$, both $(\Theta_w)_{max}$ and f Re maintain nearly constant values.

One promising avenue to manage the thermal system is to use a porous material of high conductivity, which results in large values of R_k. The impact of R_k is shown in Figure 14. It is significant to observe that $(\Theta_w)_{max}$ for type (B) can be reduced appreciably by increasing R_k, the pressure drop remains practically unchanged. This points to a new way of choosing a porous material with more desirable therophysical properties, especially a substance of high thermal conductivity. For type (A), no direct contact is made between the heat source and the porous block. Consequently, the issue of changing R_k is of little relevance to $(\Theta_w)_{max}$ for type (A), which is shown in Figure 14.

Conclusion

Wide-ranging numerical simulations to scrutinize forced convection heat transfer from a discrete heat source in a channel with porous media have been performed. The governing Navier–Stokes equations, using the Brinkman–Forchheimer-extended Darcy model for the region of porous media, were solved.

As S increases, the flow rate through the opening between the porous substrate and the channel wall is increased. A decrease of Da for a fixed value of S also causes an increase of flow rate, while the flow rate through the porous layer is decreased. For type (A), a decrease of Da results in a decrease of $(\Theta_w)_{max}$. For type (B), however, $(\Theta_w)_{max}$ increases as Da decreases. It is evident that favorable or unfavorable conditions for heat transfer exist according to the changes in S as well as in the geometric arrangement [type (A) and type (B)]. As a result, reduced $(\Theta_w)_{max}$ may be obtained by means of partially filling ($S=0.1\sim0.9$) rather than entirely filling ($S=1.0$) the channel with a porous medium, depending upon the values of S, Da, and R_k.

In view of the pressure drop, the employment of a thicker (i.e., larger S) and denser (smaller Da) porous substrate in electronic cooling equipment is less desirable.

References

Beckerman, C., Viskanta, R. and Ramadyni, S. 1988. Natural convection in vertical enclosures containing simultaneously fluid and porous layers. *J. Fluid Mech.*, **186**, 257–284

Cheng, P., Hsu, C. T. and Choudhury, A. 1988. Forced convection in the entrance region on a packed channel with asymmetric heating. *J. Heat Transfer*, **110**, 946–954

Combarnous, M. A. and Bories, S. A. 1975. Hydrothermal convection in saturated porous media. *Adv. Hydro-Science*, **10**, 231–307

Davalath, J. and Bayazitoglu, Y. 1987. Forced convection cooling across rectangular blocks. *J. Heat Transfer*, **109**, 321–327

Hadim, A. 1994. Forced convection in a porous channel with localized heat sources. *J. Heat Transfer*, **116**, 465–472

Hayase, T., Humphrey, J. A. C. and Grief, R. 1992. A consistently formulate QUICK scheme for fast and stable convergence using finite-volume iterative calculation procedures. *J. Comp. Phys.*, **98**, 108–118

Huang, P. C. and Vafai, K. 1994a. Analysis of flow and heat transfer over an external boundary covered with a porous substrate. *J. Heat Transfer*, **116**, 768–771

Huang, P. C. and Vafai, K. 1994b. Analysis of forced convection enhancement in a channel using porous blocks. *J. Thermophys. Heat Transfer*, **8**, 563–573

Hunt, M. L. and Tien, C. L. 1988. Effects of thermal dispersion on forced convection in fibrous media. *Int. J. Heat Mass Transfer*, **31**, 301–310

Incropera, F. P. 1988. Convective heat transfer in electronic equipment cooling. *J. Heat Transfer*, **110**, 1097–1111

Kang, B. H., Jaluria, Y. and Tewari, S. S. 1990. Mixed convection transport from an isolated heat source module on a horizontal plate. *J. Heat Transfer*, **112**, 653–661

Kaviany, M. 1985. Laminar flow through a porous channel bounded by isothermal parallel plates. *Int. J. Heat Mass Transfer*, **28**, 851–858

Kaviany, M. 1991. *Principles of Heat Transfer in Porous Media*, Springer, New York

Kays, W. M. and Crawford, M. E. 1980. *Convective Heat and Mass Transfer*, McGraw-Hill, New York

Kennedy, K. J. and Zebib, A. 1983. Combined free and forced convection between horizontal parallel plates: Some case studies; *Int. J. Heat Mass Transfer*, **26**, 471–474

Kim, S. Y., Sung, H. J. and Hyun, J. M. 1992. Mixed convection from multiple-layered boards with cross-streamwise periodic boundary conditions. *Int. J. Heat Mass Transfer*, **35**, 2941–2952

Kraus, A. D. and Bar-Cohen, A. 1983. *Thermal Analysis and Control of Electronic Equipment*, Hemisphere, Bristol, PA

Lauriat, G. and Prasad, V. 1989. Non-Darcian effects on natural convection in a vertical porous enclosure. *Int. J. Heat Mass Transfer*, **32**, 2135–2147

Lundgren, T. S. 1972. Slow flow through stationary random beds and suspension of spheres. *J. Fluid Mech.*, **51**, 273–299

Patankar, S. V. 1980. *Numerical Heat Transfer and Fluid Flow*, McGraw-Hill, New York

Poulikakos, D. and Bejan, A. 1985. The departures from Darcy flow in natural convection in a vertical porous layer. *Phys. Fluids*, **28**, 3477–3484

Poulikakos, D. and Renken, K. 1987. Forced convection in a channel filled with porous medium, including the effects of flow inertia, variable porosity, and Brinkman friction. *J. Heat Transfer*, **109**, 880–888

Tong, T. W. and Sharatchandra, M. C. 1990. Heat transfer enhancement using porous inserts. *Heat Transfer & Flow in Porous Media HTD*, **156**, 41–46

Vafai, K. and Huang, P. C. 1994. Analysis of heat transfer regulation and modification employing intermittently emplaced porous cavities. *J. Heat Transfer*, **116**, 604–613

Vafai, K. and Kim, S. J. 1990. Analysis of surface enhancement by a porous substrate. *J. Heat Transfer*, **112**, 700–706.

Vafai, K. and Tien, C. L. 1981. Boundary and inertia effects on flow and heat transfer in porous media. *Int. J. Heat Mass Transfer*, **24**, 195–203